Inorganic Chemistry

Article

pubs.acs.org/IC

Electrochemical, Computational, and Photophysical Characterization of New Luminescent Dirhenium–Pyridazine Complexes Containing Bridging OR or SR Anions

Alessio Raimondi,[†] Monica Panigati,*[,†] Daniela Maggioni,[†] Laura D'Alfonso,[#] Pierluigi Mercandelli,*[,‡] Patrizia Mussini,*[,§] and Giuseppe D'Alfonso[†]

[†]Department of Inorganic, Metallorganic and Analytical Chemistry "Lamberto Malatesta", Università degli Studi di Milano, and UdR INSTM of Milano, Via Venezian 21, 20133 Milano, Italy

[‡]Department of Structural Chemistry and Inorganic Stereochemistry, Università degli Studi di Milano, Via Venezian 21, 20133 Milano, Italy

[§]Department of Physical Chemistry and Electrochemistry, Università degli Studi di Milano, Via Golgi 19, 20133 Milano, Italy

[#]Department of Physics, Università di Milano-Bicocca, Piazza della Scienza 3, 20126 Milano, Italy

Supporting Information

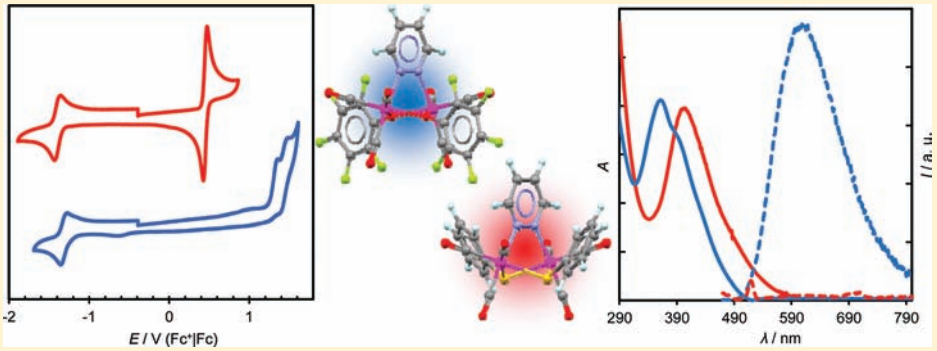

ABSTRACT: A series of $[Re_2(\mu\text{-ER})_2(CO)_6(\mu\text{-pydz})]$ complexes have been synthesized (E = S, R = C_6H_5, **2**; E = O, R = C_6F_5, **3**; C_6H_5, **4**; CH_3, and **5**; H, **6**), starting either from $[Re(CO)_5O_3SCF_3]$ (for **2** and **4**), $[Re_2(\mu\text{-OR})_3(CO)_6]^-$ (for **3** and **5**), or $[Re_4(\mu_3\text{-OH})_4(CO)_{12}]$ (for **6**). Single-crystal diffractometric analysis showed that the two μ-phenolato derivatives (**3** and **4**) possess an idealized C_2 symmetry, while the μ-benzenethiolato derivative (**2**) is asymmetrical, because of the different conformation adopted by the phenyl groups. A combined density functional and time-dependent density functional study of the geometry and electronic structure of the complexes showed that the lowest unoccupied molecular orbital (LUMO) and LUMO +1 are the two lowest-lying π^* orbitals of pyridazine, whereas the highest occupied molecular orbitals (HOMOs) are mainly constituted by the "t_{2g}" set of the Re atoms, with a strong Re−(μ-E) π^* character. The absorption spectra have been satisfactorily simulated, by computing the lowest singlet excitation energies. All the complexes exhibit one reversible monoelectronic reduction centered on the pyridazine ligand (ranging from −1.35 V to −1.53 V vs $Fc^+|Fc$). The benzenethiolato derivative **2** exhibits one reversible two-electron oxidation (at 0.47 V), whereas the OR derivatives show two close monoelectronic oxidation peaks (ranging from 0.85 V to 1.35 V for the first peak). The thioderivative **2** exhibits a very small electrochemical energy gap (1.9 eV, vs 2.38−2.70 eV for the OR derivatives), and it does not show any photoluminescence. The complexes containing OR ligands show from moderate to poor photoluminescence, in the range of 608−708 nm, with quantum yields decreasing (ranging from 5.5% to 0.07%) and lifetimes decreasing (ranging from 550 ns to 9 ns) (**3** > **4** > **6** ≈ **5**) with increasing emission wavelength. The best emitting properties, which are closely comparable to those of the dichloro complex (**1**), are exhibited by the pentafluorophenolato derivative (**3**).

INTRODUCTION

Luminescent transition-metal complexes are currently receiving much attention, because their favorable properties allow a variety of uses, particularly in the fields of bioimaging[1] and electroluminescent devices.[2]

Rhenium carbonyl-diimine complexes, $[Re(CO)_3(N,N)L]$, exhibit photoluminescence from triplet metal-to-ligand-charge transfer (^{3}MLCT) excited states, which can be widely tuned by variations of the ancillary L ligands or of the substituents on the diimine ligand,[3] attaining, in some cases, very high photoluminescence quantum yields (PLQY).[4] The presence of a

Received: October 21, 2011
Published: February 23, 2012

   dx.doi.org/10.1021/ic202284a | *Inorg. Chem.* 2012, 51, 2966–2975

single electron-accepting diimine ligand, which removes the problem of the excited-state localization that is ever-present in other polypyridine systems, makes the rhenium(I) complexes among the more-investigated organometallic systems, useful also for fundamental studies.[5]

We are currently developing a new family of luminescent rhenium(I) complexes, with the general formula $[Re_2(\mu\text{-}X)_2(CO)_6(\mu\text{-}1,2\text{-diazine})]$ (where X = hydrides[6] or halides;[7,8] see Chart 1). Wavelengths, lifetimes, and quantum yields of the

Chart 1

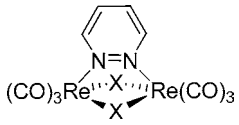

emission dramatically vary upon varying the diazine substituents and the ancillary ligands X.[6−8] The derivatives with X = Cl and two alkyl groups in the β positions of the diazine give the highest PLQYs, up to 0.53 in toluene solution at room temperature.[8] By contrast, the presence of substituents in the α positions nearly zeroes the emission, because of steric hindrance with the carbonyl ligands, which reduces the stiffness of the complex, promoting nonradiative deactivation pathways.[7] The replacement of chlorides by bulkier bromides and iodides also freezes the emission (in solution at room temperature),[7] in agreement with the decreased rigidity of the coordination sphere upon increasing the bulkiness of the bridging ligands.

Therefore, we decided to investigate the photophysical properties of diazine complexes bearing polyatomic bridging ligands, with a twofold objective. First, we were interested in learning how to exploit changing the ancillary ligands to control the highest occupied molecular orbital−lowest unoccupied molecular orbital (HOMO−LUMO) gap, and then modulating the position and intensity of the emission. Moreover, the raising of the HOMO level could give low-band-gap complexes, which are of interest for efficient light harvesting in solar cells.

Second, the replacement of chlorides by polyatomic ligands might also provide other sites, besides the diazine ring, for functionalizing the dirhenium complexes, which might be useful for application as luminescent bioprobes, where the linking to suitable biomolecules is most-often required.

Here, we report on the synthesis and on the electrochemical, computational, and photophysical characterization of five new $[Re_2(\mu\text{-}ER)_2(CO)_6(\mu\text{-pydz})]$ complexes, containing pyridazine (pydz) as a chromophoric ligand and ER^- groups as bridging ancillary ligands (E = S, R = C_6H_5, **2**; E = O, R = C_6F_5, **3**; C_6H_5, **4**; CH_3, and **5**; H, **6**).

RESULTS AND DISCUSSION

Synthesis of the New Complexes. The previously reported $[Re_2(\mu\text{-}Cl)_2(CO)_6(\mu\text{-pydz})]$ complex **1**, as well as all the other complexes $[Re_2(\mu\text{-}X)_2(CO)_6(\mu\text{-}1,2\text{-diazine})]$ (X = Cl, Br, I), were obtained by refluxing the proper $[Re(CO)_5X]$ starting material with the stoichiometric amount of 1,2-diazine. This method cannot be used for the preparation of the title derivatives, since $[Re(CO)_5(OR)]$ complexes are unstable and elusive species.[9] Therefore, we developed alternative routes, using different starting materials, as summarized in Scheme 1.

In a first approach, the $[Re(CO)_5(OTf)]$ complex,[10] containing the labile triflate $CF_3SO_3^-$ anion (OTf^-), was used. The complex was treated with the proper REH reagent (E

Scheme 1. The Different Synthetic Routes (i−v) Leading to Complexes 1−6

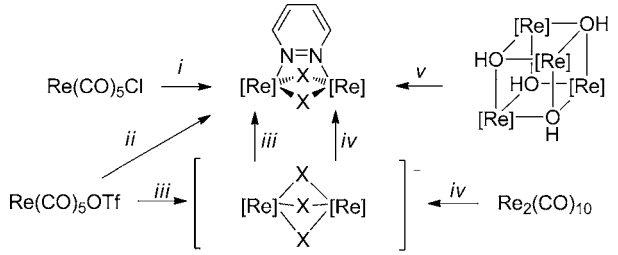

[Re] = $Re(CO)_3$; *i*: **1**; *ii*: **2**, **4**; *iii*: **3**; *iv*: **5**; *v*: **6**

X = Cl (**1**); = SC_6H_5 (**2**); = OC_6F_5 (**3**); = OC_6H_5 (**4**); = OCH_3 (**5**); = OH (**6**)

= O or S) and stoichiometric pyridazine (pydz), in the presence of a base B, according to eq 1.

$$2[Re(CO)_5(OTf)] + pydz + 2REH + 2B \rightarrow [Re_2(\mu\text{-}ER)_2(CO)_6(\mu\text{-pydz})] + 2BH^+OTf^- + 4CO \quad (1)$$

Bis(dimethylamino)naphthalene (DMAN) was chosen as base, because it cannot compete with diazine for rhenium coordination.

This route worked satisfactorily with C_6H_5SH, in THF solution, and gave the bis(thiophenolato) derivative $[Re_2(\mu\text{-}SC_6H_5)_2(CO)_6(\mu\text{-pydz})]$ (**2**) in ca. 30% isolated yields. In the case of C_6H_5OH, reaction 1 also worked, but cleanly gave $[Re_2(\mu\text{-}OC_6H_5)_2(CO)_6(\mu\text{-pydz})]$ (**4**), using only molten phenol as a solvent.

In contrast, attempts to obtain the bis(pentafluorophenolato) derivative $[Re_2(\mu\text{-}OC_6F_5)_2(CO)_6(\mu\text{-pydz})]$ (**3**) with the same procedure afforded a mixture of products in which the expected derivative was present in relatively low concentration (<30% from ^1H NMR analysis). Then, **3** was better obtained via a two-step procedure. At first, the dinuclear anion $[Re_2(\mu\text{-}OC_6F_5)_3(CO)_6]^-$ was formed, by reacting $[Re(CO)_5(OTf)]$ with pentafluophenol in the presence of a base (B = DMAN, see eq 2a), then the anion was treated with 1 equiv of pydz, resulting in the replacement of one phenolate by a diazine molecule (see eq 2b).

$$2[Re(CO)_5(OTf)] + 3C_6F_5OH + 3B \rightarrow [Re_2(\mu\text{-}OC_6F_5)_3(CO)_6]^- + 4CO + 3HB^+ + 2OTf^- \quad (2a)$$

$$[Re_2(\mu\text{-}OC_6F_5)_3(CO)_6]^- + pydz \rightarrow [Re_2(\mu\text{-}OC_6F_5)_2(CO)_6(\mu\text{-pydz})] + C_6F_5O^- \quad (2b)$$

To prepare the $[Re_2(\mu\text{-}OCH_3)_2(CO)_6(\mu\text{-pydz})]$ species (**5**), we used the dinuclear $[Re_2(\mu\text{-}OCH_3)_3(CO)_6]^-$ anion directly as starting material, which can be prepared in good yields, as NEt_4^+ salt, from the reaction of $[Re_2(CO)_{10}]$ with bases.[11] Differently from the bis(pentafluorophenolato) derivative, in this case, the addition of 1 equiv of triflic acid was necessary to

dx.doi.org/10.1021/ic202284a | Inorg. Chem. 2012, 51, 2966−2975

promote the elimination of one of the bridging methoxo groups (see eq 3).

$$[Re_2(\mu\text{-}OCH_3)_3(CO)_6]^- + pydz + TfOH \rightarrow [Re_2(\mu\text{-}OCH_3)_2(CO)_6(\mu\text{-}pydz)] + CH_3OH + OTf^- \quad (3)$$

This agrees with the higher nucleophilicity and lower bulkiness of OCH_3^-, with respect to $OC_6F_5^-$.

Finally, a still different method was developed to prepare the hydroxo $[Re_2(\mu\text{-}OH)_2(CO)_6(\mu\text{-}pydz)]$ derivative (**6**). The cubane-like $[Re_4(\mu_3\text{-}OH)_4(CO)_{12}]$ complex[12] (Scheme 1) was used as starting material, and it was reacted with 2 equiv of pydz, in water solution and under microwave activation, resulting in the clean formation of **6**, according to eq 4.

$$[Re_4(\mu_3\text{-}OH)_4(CO)_{12}] + 2pydz \rightarrow 2[Re_2(\mu\text{-}OH)_2(CO)_6(\mu\text{-}pydz)] \quad (4)$$

This reaction resembles the previously reported fragmentation of the unsaturated tetranuclear cluster $[Re_4(\mu_3\text{-}H)_4(CO)_{12}]$ with 2 equiv of pydz,[6] even if, in this case, only the [2 + 2] fragmentation pathway was observed, quantitatively affording the dinuclear saturated derivative **6**.

The nature of the reaction products was unambiguously established by the spectroscopic and analytical characterization, and confirmed by the X-ray analysis of complexes **2**, **3**, and **4**. All the products exhibit in the ν(CO) regions of the IR spectra the four bands pattern typical of this class of compounds,[7] with a shift to low wavenumbers upon increasing the donor power of the bridging ligand (this point will be better discussed below).

The ^{1}H NMR data agree with the expected structures. In particular, the two resonances of the bridging pyridazine are downfield shifted by ~0.5−0.6 ppm, with respect to the free ligand, as observed in related complexes.[7]

Variable-temperature ^{19}F NMR spectra gave some information on the solution structure and dynamics of complex **3**. The low-temperature (T < 221 K) spectra are consistent with the C_2 solid-state structure (see below), with five different signals for the five fluorine atoms of the two (equivalent) pentafluorophenolato groups. The chemical-shift difference between the two *ortho* resonances (>5 ppm) is much larger than that between the two *meta* resonances (<1 ppm), because of the shielding effect of the diazine π-electrons on one of the *ortho* F atoms, as evidenced by the ^{1}H−^{19}F HOESY experiment shown in Figure S1 in the Supporting Information. Upon increasing the temperature, the *ortho* and *meta* signals broadened (see Figure S2 in the Supporting Information), indicating the rotation of each C_6F_5 ring around the C−O axis, leading to equalization of the two *ortho* and two *meta* positions. Band shape analysis on the ^{19}F spectra provided the value of the activation energy for this process (42.4 kJ mol^{-1}). In the case of the phenolato derivative (**4**), the ^{1}H NMR spectra did not show either splitting or broadening of the *ortho* and *meta* signals upon reducing the temperature, indicating that the rotation of the C_6H_5 rings is faster than that of their C_6F_5 counterparts, because of the lower steric hindrance with the CO ligands.

Solid-State Structures. The crystal structures of the μ-benzenethiolato derivative (**2**) and of the two μ-phenolato derivatives (**3** and **4**) have been determined. Figure 1 shows frontal and lateral views of the two complexes **2** and **3**; the structure of **4** is depicted in the Supporting Information (Figure S3).

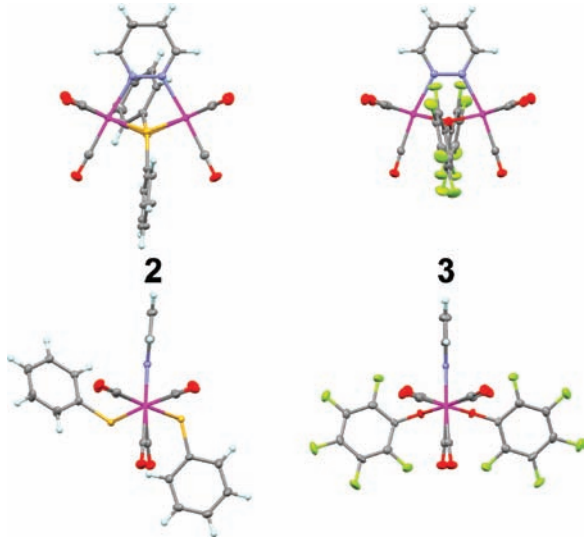

Figure 1. Crystal structures of $[Re_2(\mu\text{-}SC_6H_5)_2(CO)_6(\mu\text{-}pydz)]$ (**2**) and $[Re_2(\mu\text{-}OC_6F_5)_2(CO)_6(\mu\text{-}pydz)]$ (**3**): frontal and lateral views (upper line and lower line, respectively). Displacement ellipsoids are drawn at the 50% probability level. (Color code: C, gray; H, white; F, lime green; N, blue; O, red; Re, magenta; and S, yellow.)

In these dinuclear species, each Re atom attains a distorted octahedral coordination and bears three terminal carbonyl ligands in a facial arrangement, one of the N atoms of the bridging pyridazine ligand, and the S (or O) atoms of the two bridging benzenethiolato (or phenolato) ligands. The two μ-phenolato derivatives **3** and **4** possess an idealized C_2 symmetry (although only **3** lies on a crystallographic 2-fold axis), while the thio-derivative **2** is asymmetrical, because of the different conformation adopted by the phenyl groups of the two bridging benzenethiolato ligands.

Despite the smaller Re−S−Re bond angle in **2** (91.0°), with respect to the corresponding Re−O−Re angles in **3** and **4** (104.4 and 103.8°), the Re−Re distance is much longer in the sulfur-containing derivative (3.57 Å in **2** vs 3.39 and 3.35 Å in **3** and **4**), as a consequence of the larger covalent radius of sulfur, compared to oxygen. The Re−S bond distance in **2** (2.50 Å) is indeed ca. 0.35 Å longer than the Re−O bond distances in **3** and **4** (2.15 and 2.13 Å).[13]

The coordination geometry of the O atoms of the μ-phenolato ligands is almost exactly planar (sum of the bond angles: 359.9° and 358.8° in **3** and **4**), suggesting the presence of a partial double bond character in the Re−O bonds. In contrast, the S atoms of the μ-benzenethiolato ligands in **2** show a pyramidal geometry (sum of the bond angles: 314.6°). As a consequence, the phenyl substituents in the thio-derivative **2** are not constrained to lie in the plane defined by the Re−(μ-S)−Re atoms, leading to the possible existence of geometric isomers in which the phenyl groups are directed either toward or away from the μ-pyridazine ligand. Both the orientations can be observed in the molecular conformation adopted by the molecule in the solid state (see the lateral view of **2** in Figure 1). However, the presence in solution of other (more symmetrical) isomers can be foreseen.

Computational Study. The new rhenium complexes **2**−**6** were studied by means of density functional and time-dependent density functional (TD-DFT) computations. The

dx.doi.org/10.1021/ic202284a | Inorg. Chem. 2012, 51, 2966−2975

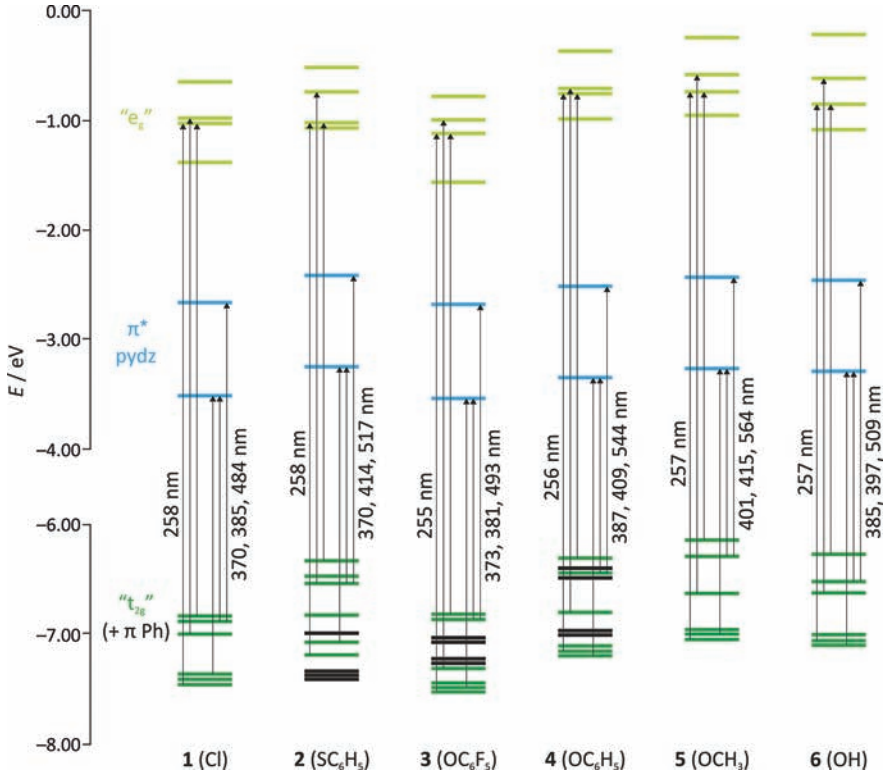

Figure 2. Partial molecular orbital diagram for the complexes $[Re_2(\mu\text{-}X)_2(CO)_6(\mu\text{-pydz})]$, X = Cl (**1**), SC_6H_5 (**2**), OC_6F_5 (**3**), OC_6H_5 (**4**), OCH_3 (**5**), and OH (**6**). Orbitals are colored according to their main component: rhenium "t_{2g}" orbitals (dark green), pyridazine π^* orbitals (light blue), rhenium "e_g" orbitals (light green), and phenyl π orbitals (black, in complexes **2**−**4**). Arrows correspond to electronic transitions involved in the absorption spectra (computed TD-DFT wavelengths are given). In particular, for each species, values on the left and the right refer to the d−d and the MLCT absorption, respectively.

optimized structures of complexes **3**−**6** possess the highest possible symmetry for these species (C_{2v}), while the benzenethiolato derivative **2** belongs to the C_2 point group.[14] As already found for **1**,[7,8] LUMO and LUMO+1 are the two lowest-lying π^* orbitals of the coordinated pyridazine. The following four MO (from LUMO+2 to LUMO+5) are the "e_g" set of the two Re atoms, showing, in addition, a large C≡O π^* character.

For species **5** and **6**, the six HOMOs are the "t_{2g}" set of the two Re atoms in a pseudo-octahedral environment. In particular, the three highest-lying orbitals show a strong Re−(μ-O) π^* character, in close analogy with the halogenated derivatives previously described.[7] For species **2**−**4**, ten HOMOs must be taken into account, since the energy of the "t_{2g}" orbitals of the Re atoms is similar to those of the four highest-lying π orbitals of the two phenyl groups of the phenolato (or pentafluorophenolato) bridging ligands. For species **2**, in addition, a partial mixing of these two types of MO is observed and some of the "t_{2g}" orbitals are partially delocalized over the phenyl moieties. Molecular orbital energies are listed in Table S1 in the Supporting Information and partial orbital diagrams are depicted in Figure 2. A views of the most relevant molecular orbitals for complex **6** is reported in Figure S4 in the Supporting Information, while a comparison of the HOMOs of species **1**, **2**, **4**, and **6** can be found in Figure S5 in the Supporting Information.

In all the species but **2**, the HOMO is a totally symmetric orbital, analogous to those previously found in the halogenated derivatives.[7] The HOMO of **2** has a very similar composition; however, it is antisymmetric, with respect to the C_2 axis.

The absorption spectrum of all the complexes, down to 230 nm, was simulated by computing the lowest 50 singlet excitation energies. Selected transitions are reported in Table S2 in the Supporting Information and depicted in Figure 2. The results will be discussed in the section Photophysical Characterization.

Electrochemical Characterization. Figure 3 shows the results of cyclic voltammetry (CV) analyses of complexes **2**−**6** in acetonitrile solution, including, for comparison, the previously published data concerning the dichloro complex **1** and the analogous dibromo and diiodo derivatives, that hereafter will be indicated as **1′** and **1″**, respectively.[7] The most significant CV features are reported in Table 1, while a more-extensive selection of the CV data is provided in Table S3 of the Supporting Information, where the voltammograms recorded in CH_2Cl_2 solution also are reported (see Figure S6 in the Supporting Information).

First Reduction Peaks. The first reduction peaks must be localized for all complexes on their common pyridazine ligand, consistent with our previous work.[7] Accordingly, such peaks are quite similar for all complexes, both in shape and potential, while they strongly differ from the free ligand one. In fact, the first reduction peak of pyridazine, located at a very negative potential (−2.6 V vs $Fc^+|Fc$), is chemically irreversible and accounts for an uptake of two electrons,[7] while the first reduction peaks of the complexes are much more positive (by 1.05−1.25 V), implying that the coordination makes the diazine ligand much more electron-poor. Moreover, the reduction of all complexes is monoelectronic and reversible, both from the chemical point of view (symmetrical return peaks, stable

dx.doi.org/10.1021/ic202284a | Inorg. Chem. 2012, 51, 2966−2975

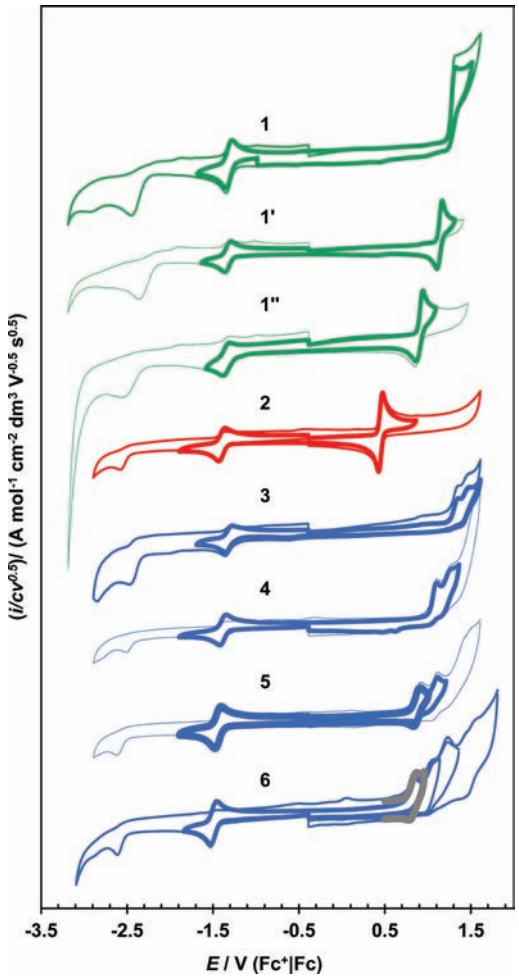

Figure 3. Normalized CV features for the complexes investigated in this work and the three complexes with halide ligands previously investigated **1**, **1′**, **1″** (green lines),[7] recorded on a glassy carbon (GC) electrode at 0.2 V s^{-1} in acetonitrile solution. The gray line for **6** refers to a scan at 2 V s^{-1}.

product) and the electrochemical one (facile transfer of a single electron, which is taken into account by the ∼57 mV half-peak widths together with the almost-zero E_p versus log ν slopes), thus accounting for very fast formation of a stable radical anion (see Table S3 in the Supporting Information). The normalized convoluted peak currents (see the Experimental Section) regularly decrease with increasing bulkiness of the X ligands, in agreement with the regular decrease of the diffusion coefficients of the investigated complexes.

The radical anion formation seems to be significantly favored by the more-polar CH_3CN solvent, with respect to CH_2Cl_2, in both thermodynamic and kinetic terms, since the normalized reduction potentials are significantly less negative, and the electrochemical reversibility criterion ($E_p - E_{p/2} \approx 0.057$) are met much more strictly (see Table S3 in the Supporting Information).

First Oxidation Peaks. In our former study on dirhenium–diazine complexes with halide ancillary ligands,[7] the first oxidation site was found to be localized on the metal core, and the corresponding oxidation peak to be chemically and electrochemically reversible and bielectronic, pointing to simultaneous two-electron loss from the dinuclear metal core. In contrast, in the series of the OR derivatives reported here (**3**–**6**), a close sequence of two monoelectronic peaks is observed (the number of exchanged electrons being confirmed by comparison of the oxidation limiting currents with the reduction ones; see Table S3 in the Supporting Information). The first peak tends to chemical irreversibility at low scan rates (no return peak, half-peak widths lower than in the reversible case, consistent with an EC mechanism), while chemical reversibility improves with increasing scan rate, at least in the OCH_3 and OH complexes **5** and **6** (see, for instance, the gray curve in the OH case in Figure 3, corresponding to 2 V s^{-1}). The much more pronounced reversibility for the OCH_3 derivative **5**, qualitatively recognizable in Figure 3, has been confirmed by the quantitative estimate of the pseudo-first-order rate constants (k') for the chemical reaction of the product of the first monoelectronic oxidation step (see the Experimental Section and Figure S7 in the Supporting Information). In contrast, the two phenolato derivatives **3** and **4** show a combination of an irreversible first peak followed by a reversible second peak, in the entire scan rate range explored. These features resemble the usual oxidative CV patterns of alkyl–aryl ethers,[15] although it could be only a coincidence.

The picture described here seems to be strictly connected to the presence of bridging O atoms. Indeed, the SC_5H_6 derivative **2** shows (in both of the investigated solvents) the reversible, bielectronic oxidation peak already observed in the halide cases. Another surprising feature of **2** is the value of its oxidation potential (0.47 V), which is much lower than that of the phenolato derivative (**4**) (1.1 V), despite the close similarity of their HOMO energies (see Figure 2 and Table S1 in the Supporting Information). Figure 4a shows a plot of the E_p values (for compounds **2**–**6** and the related halide derivatives **1**,

Table 1. Selected CV Features[a] for the $[Re_2(\mu\text{-}X)_2(CO)_6(\mu\text{-pydz})]$ Complexes Investigated Here and in a Previous Work (ref 7)

compound	X	F	R	$E_{p\ max,\ red}$ [V]	$E_{p\ max,\ I\ ox}$ [V]	$E_{p\ max,\ II\ ox}$ [V]	LUMO [eV]	HOMO [eV]	E_g [eV]
1[b]	Cl	0.42	−0.19	−1.345	1.315		−3.46	−6.12	2.66
1′[b]	Br	0.45	−0.22	−1.365	1.163		−3.44	−5.96	2.53
1″[b]	I	0.42	−0.24	−1.378	0.944		−3.42	−5.74	2.32
2	SC_6H_5	0.30	−0.23	−1.431	0.473		−3.37	−5.27	1.90
3	OC_6F_5	n.a.	n.a.	−1.352	1.345	1.463	−3.45	−6.15	2.70
4	OC_6H_5	0.37	−0.40	−1.416	1.100	1.254	−3.38	−5.90	2.52
5	OCH_3	0.29	−0.56	−1.475	0.911	1.114	−3.33	−5.71	2.39
6	OH	0.33	−0.70	−1.527	0.854	1.070	−3.27	−5.65	2.38

[a]Peak potentials E_p (scan rate = 0.2 V s^{-1}); electrochemical HOMO and LUMO energy levels and gaps calculated along the peak maxima. Potentials are referred to the $Fc^+|Fc$ couple in the operating media (MeCN + 0.1 M $TBAPF_6$). Values of the Swain–Lupton parameters F and R are also provided for each group X. [b]Data taken from ref 7.

dx.doi.org/10.1021/ic202284a | Inorg. Chem. 2012, 51, 2966–2975

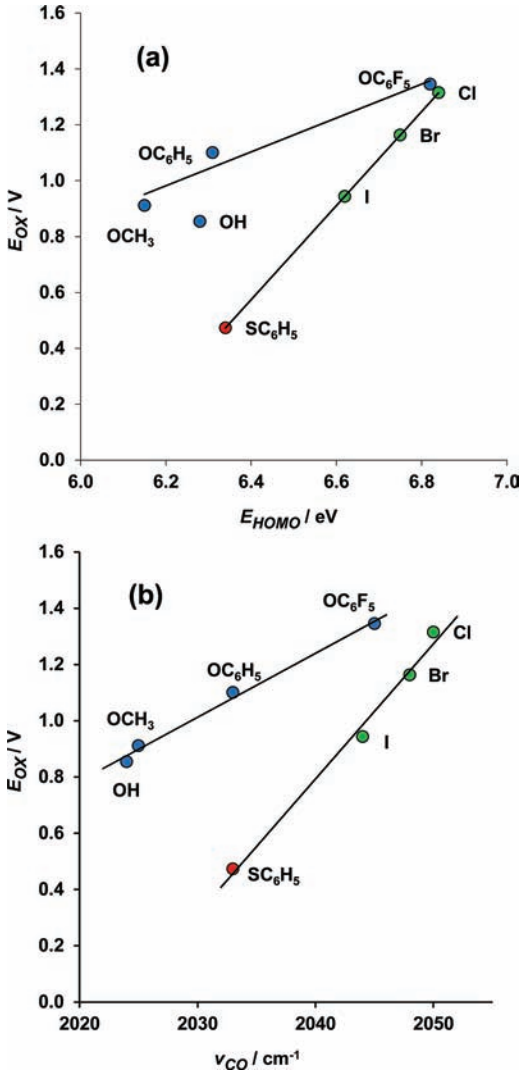

Figure 4. Plot of the first oxidation E_p values (measured in acetonitrile solution) versus (a) the vacuum computed HOMO energies and (b) the wavenumbers of the highest energy (totally symmetric) ν(CO) band (acetonitrile solution).

1′, and **1**″)[7] versus the energies computed for the HOMO in vacuo. Two trends can be clearly recognized (except the aberrant behavior of the μ-hydroxo species **6**, attributable to the presence of specific hydrogen bond interactions with the solvent that are not described by the calculation). The sulfur derivative **2** perfectly fits with the trend of the complexes bearing halide ancillary ligands, while the phenolato **4** agrees with the trend of the OR derivatives.

An impressively similar two-trend plot (Figure 4b) is obtained by correlating the measured oxidation potentials with the ν(CO) values of the stretching modes, which are reliable indicators of the electron density on the metal atom. In this second correlation, both of the plotted quantities have been measured in solution and then, in this case, the OH derivatives **6** also fit the trend of the other OR species.

A similar correlation (see Figure S8 in the Supporting Information) also is obtained by evaluating the variation of the oxidation potentials versus one (R) of the two descriptors of the substituents effects in organic reactions, developed by Swain and Lupton for factoring the Hammett's σ constants into its inductive and resonance components (the F and R parameters, respectively).[16]

These findings fully support the view that the oxidation process is markedly different in the case of the oxygen-bridged derivatives (which show two monoelectronic oxidation steps), with respect to the other four complexes, which exhibit a single bielectronic oxidation step. This might be related to the closer Re(μ-X)$_2$Re scaffold and to the harder nature of the bridging ligands in the case of the OR derivatives, which could result in a less-efficient stabilization of the cationic products, with respect to the softer anions. A detailed mechanistic electrochemical investigation will be necessary to throw light into this point.

The last column of Table 1 shows the electrochemical HOMO−LUMO gap. The energy gap for the SR derivative **2** is, by far, the smallest in the series (lower than 2 eV, both along the maxima and the onset criteria; see Table S3 in the Supporting Information for the latter value), while the highest energy gap is obtained, as expected, with the OC_6F_5 ligand, which approximately corresponds to the chloride case in the halide series. Actually, the effects of Cl and OC_6F_5 ligands seem to be almost equivalent, from a thermodynamic point of view (almost equal HOMO and LUMO levels and first oxidation and reduction potentials, albeit the oxidative reaction mechanism is different).

Photophysical Characterization. At room temperature, in dichloromethane solution, all the complexes show spectra dominated by two main absorption features in the ultraviolet−visible (UV−vis) region (see Figure S9 in the Supporting Information and Figure 5 for complex **3** in different solvents).

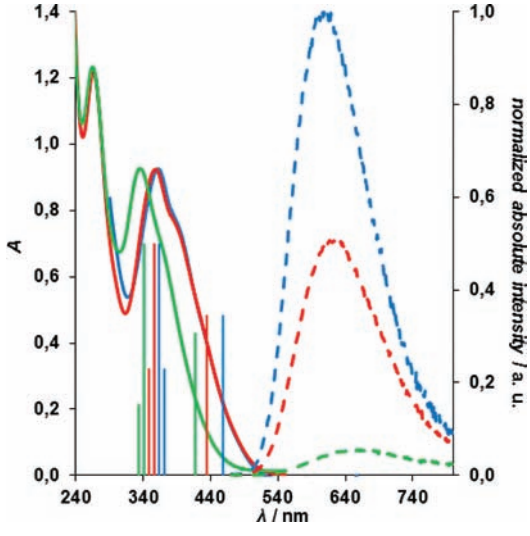

Figure 5. Solvent effect on the absorption (—) and emission (- - -) spectra of [$Re_2(\mu$-$OC_6F_5)_2(CO)_6(\mu$-pydz)] (**3**). A comparison with the computed excitation energies and oscillator strengths (vertical lines) is reported. (Color legend: blue, toluene; red, dichloromethane; green, acetonitrile.)

On the basis of the TD-DFT computations, the bands at higher energy, whose position (ca. 270 nm) is independent of the polarity of the solvent, can be attributed to the superposition of many singlet d−d excitations from the "t_{2g}" set to the "e_g" set of the two Re atoms. Some π−π* excitations of the pyridazine ligand fall in the same range of energy (230−300 nm); however, their transition probabilities are significantly lower than those of the d−d ones (at least for the transitions lying in the energetic range considered in the computational study). In

dx.doi.org/10.1021/ic202284a | Inorg. Chem. 2012, 51, 2966−2975

Table S2 in the Supporting Information (and in Figure 2), only the most-intense transition of A_1 (or A) symmetry is reported. Conductor-like polarizable continuum model (CPCM) calculations confirm that these transitions are almost unaffected by the solvent.

The lower-energy absorption bands, which have a slightly lower intensity, can be assigned to metal−ligand-to-ligand charge transfer (MLLCT) transitions, taking into account the significant contribution of the bridging ancillary ligands to the metal-centered HOMO set. These bands arise from the convolution of multiple transitions, as testified by the more- or less-pronounced shoulders observed at lower frequencies. In particular, the three transitions (from HOMO−n to LUMO or LUMO+1 orbitals) already described for the halogenated derivatives[7] can also be identified for the new species **2**−**6**, and are listed in Table S2 in the Supporting Information (and in Figure 2). The computed wavelengths are in fair agreement with the experimental absorption maxima measured in a toluene solution. The mean absolute deviation between the experimental λ_{max} and the wavelength for the more-intense totally symmetric excitation computed in the gas phase is 24 nm. The agreement strongly improves (the mean absolute deviation reduces to 9 nm) by including the toluene solvent in the calculation.

The charge-transfer character of such transitions is supported by their strong solvent dependence:[17] indeed, as already reported for the related $Re_2(\mu$-diazine) complexes,[6−8] a blue shift is observed upon increasing solvent polarity (for instance, from 363 nm in toluene to 335 nm in MeCN for **3**; see Figure 5).

Upon excitation at 450 nm (for **2**−**4**) or 480 nm (for **5** and **6**), at room temperature in diluted deoxygenated toluene solutions, all the complexes with bridging OR groups show broad, featureless emission in the red region of the visible spectrum (range of 608−708 nm). The photoluminescence spectra for complexes **3**−**6** are shown in Figure 6, and the data are summarized in Table 2.

It has been checked that the emission is independent of the excitation wavelength and that all the complexes are photostable. On the basis of previous results on related systems, the emission can be confidently described as arising from triplet metal-to-ligand charge transfer (^{3}MLCT) states, as supported by the red shift (for **3**: λ_{em} = 608 nm in toluene, 620 nm in dichloromethane, 650 nm in acetonitrile) and the strong decrease of the emission intensity observed upon increasing the solvent polarity (see Figure 5 for **3**).

The photophysical properties of the pentafluorophenolato derivative **3** are closely comparable to those of the parent dichloro-derivative **1** (see Table 2), in agreement with the close similarity of their HOMO and LUMO levels, and then of their reduction and oxidation potentials. The position of the emission of the four complexes **3**−**6** is strongly affected by the nature of the OR groups and red shifts upon increasing the donor power of the ligand, following the trend of the electrochemical HOMO−LUMO gaps. The photoluminescence quantum yields decrease in the same order (see Table 2 and Figure 6), according to the Energy Gap Law (EGL), and the k_{nr} values roughly lie on the same line as the previously reported dichloro derivatives containing pydz, monoalkylpyridazines, and dialkylpyridazines (see Figure S10 in the Supporting Information). This indicates that the nature of the excited states and the pathways responsible for their nonradiative deactivation are only slightly affected by the nature of the bridging ancillary X ligands, provided that these do not perturb the stiffness of the $Re_2(\mu$-X$)_2(\mu$-diazine) core (as it occurs with the bulky Br derivative, whose k_{nr} value falls well above the EGL line).

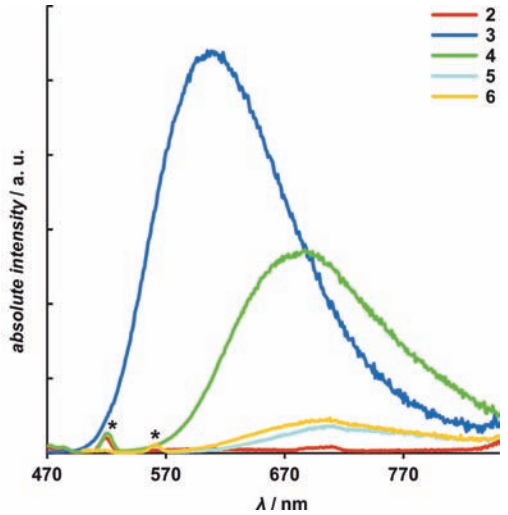

Figure 6. Effect of the ancillary OR or SR ligands on the emission spectra, recorded at room temperature in deoxygenated toluene solution, upon excitation at 450 nm (for **2**−**4**) or 480 nm (for **5** and **6**). The emission intensity of the OC_6F_5 derivative **3** has been decreased by a factor of 5 relative to the other complexes. Bands indicated with * are artifacts due to the Raman scattering from the toluene solvent.

It is worth mentioning that complexes containing analogous $Re_2(\mu$-ER$)_2(CO)_6$ fragments (E = O, S), joined by 4,4′-bipyridil ligands in $[Re_2(\mu$-ER$)_2(CO)_6(4,4'$-bpy$)_2]_2$ molecular rectangles, had been previously reported,[18] and also in these cases (very weak) emission in solution was observed only from some of the OR derivatives (highest PLQY 0.039% in acetonitrile solution).[18d]

CONCLUSIONS

The synthesis of a series of neutral dinuclear rhenium complexes of general formula $[Re_2(\mu$-ER$)_2(CO)_6(\mu$-pydz$)]$ (E = O or S) has been performed. Several new synthetic routes have been developed, all of which are more complex than those used for the related dihalogen $[Re_2(\mu$-X$)_2(CO)_6(\mu$-1,2-diazine$)]$ complexes, because of the unavailability of $[Re(CO)_5X]$ starting materials when X = ER.

The substitution of halides by OR groups does not modify significantly the nature of the frontier orbitals and of the absorption/emission processes, which maintain the previously described metal−ligand-to-ligand charge transfer character. The bridging OR groups are deeply involved in the HOMO set, whose energy progressively rises on increasing the OR donor power (except the deviant behavior of the OH derivative), with consequent easier oxidation of the complex and reduced band gap. Accordingly, a progressively red-shifted and weakened emission is observed upon going from OC_6F_5 to OC_6H_5 to OCH_3 (and OH).

These results confirm that it is possible to modulate the photophysical properties of the Re_2-diazine complexes in a twofold manner: the variation of the substituents on the chromophoric moiety (the diazine ring) affects the LUMO level, while the variation of the ancillary ligands modifies the HOMO level.

dx.doi.org/10.1021/ic202284a | Inorg. Chem. 2012, 51, 2966−2975

Table 2. Absorption and Emission Data in Toluene Solution of $[Re_2(\mu\text{-}X)_2(CO)_6(\mu\text{-pydz})]$ Complexes

compound	X	λ_{abs} [nm]	ε [$\times 10^{-3}$ M^{-1} cm^{-1}]	λ_{em} [nm]	Φ_{em} [$\times 10^{2}$]	τ [ns]	k_r [$\times 10^{-5}$ s^{-1}]	k_{nr} [$\times 10^{-5}$ s^{-1}]
1[a]	Cl	379	8.1	603	7.0	800	0.88	11.6
2	SC_6H_5	403	7.0					
3	OC_6F_5	362	7.6	608	5.5	550	1.0	17.2
4	OC_6H_5	374	6.9	680	0.55	37	1.5	270
5	OCH_3	372	8.7	708	0.07	8.6	0.81	1160
6	OH	369	8.0	702	0.09	9.2	0.98	1090

[a]The data for the Cl derivative are taken from the Supporting Information in ref 19.

The behavior of the bis-pentafluorophenolato complex **3** is comparable to that of the dichloro complex **1**; therefore, improvement in the photoluminescence quantum yields is expected upon raising the LUMO levels, by replacing pyridazine with the 4,5-dialkyl-pyridazine ligands, as previously observed in the series of dichloro derivatives.[8]

However, a perfluorophenolate unit is of limited interest for bioconjugation. Therefore, the low emission properties of the complexes bearing OR groups different from OC_6F_5, together with the not-straightforward synthesis of this family of $[Re_2(\mu\text{-}OR)_2(CO)_6(\mu\text{-pydz})]$ complexes, indicate that this approach might not be ideal for conjugating a luminescent Re_2-diazine group to biomolecules bearing ROH moieties. Different routes will be investigated, involving inter alia mixed $[Re_2(\mu\text{-Cl})(\mu\text{-OR})(CO)_6(\mu\text{-diazine})]$ derivatives, which are expected to exhibit higher PLQYs than the corresponding bis-(OR) derivatives. Moreover, the strong enhancement of the luminescence on going from organic to aqueous solution, exhibited by some $[Re_2(\mu\text{-OR})_2(CO)_6(4,4'\text{-bpy})_2]_2$ rectangles bearing long alkyl chains,[18d] suggests that analogous self-aggregation phenomena might positively perturb the emissive behavior of our systems when bonded to large biomolecules.

As far as the benzenethiolate derivative (**2**) is concerned, despite its lack of luminescent properties, it appears to be of interest, from a different point of view. Its low energy band gap and its perfectly reversible oxidation and reduction processes might find application for current generation by light harvesting. We are currently investigating the modulation of the electrochemical and light absorption properties of similar $[Re_2(\mu\text{-SR})_2(CO)_6(\mu\text{-1,2-diazine})]$ complexes upon varying the nature of the SR groups and of the diazine substituents.

EXPERIMENTAL SECTION

All of the reactions were performed under N_2, using the Schlenk technique and solvents deoxygenated and dried by standard methods. Pyridazine (pydz) was used as received from Aldrich. $[Re(CO)_5(OTf)]$,[10] $NEt_4[Re_2(\mu\text{-}OCH_3)_3(CO)_6]$,[11] and $[Re_4(\mu_3\text{-}OH)_4(CO)_{12}]$[12] were prepared according to literature methods. Elemental analyses were carried out in the Department of Inorganic, Metallorganic and Analytical Chemistry of the University of Milan. EI-HRMS were acquired on a VG Autospec M246 spectrometer. ^1H and ^{19}F NMR spectra were recorded on Bruker DRX300 or DRX400 spectrometers. IR spectra were acquired on Bruker Vector22 FT instrument. Electronic absorption spectra were recorded on Agilent 8543 spectrophotometer, at room temperature.

Synthesis of $[Re_2(\mu\text{-}SC_6H_5)_2(CO)_6(\mu\text{-pydz})]$ (2). A sample of $[Re(CO)_5(OTf)]$ (50 mg, 0.105 mmol) dissolved in freshly distilled THF was treated with 0.5 equiv of pyridazine (4.2 mg, 0.053 mmol) and then with 1 equiv of C_6H_5SH (12 mg, 0.105 mmol) and 1 equiv of bis(dimethylamino)naphthalene (DMAN) (22.9 mg, 0.105 mmol). The reaction mixture was refluxed for 2.5 h. A white precipitate was separated and the supernatant solution was evaporated to dryness. Separation by column chromatography on SiO_2 using ethyl acetate/dichloromethane 1:19 afforded spectroscopically pure **2** (R_F = 0.90). Isolated yield: 13 mg, 30%. IR ν(CO) (cm^{-1}), CH_2Cl_2: 2035 w, 2018 s, 1936 m, 1912 m. ^1H NMR (δ, CD_2Cl_2): 9.96 (pseudo t, 2H), 7.90 (pseudo t, 2H), 7.18−7.12 (m, 10H). UV−vis (CH_2Cl_2) λ = 406 nm (6.8×10^3 cm^{-1} M^{-1}). Anal. Calcd: C, 31.50; H, 1.68; N, 3.34. Found: C, 31.42; H, 1.74; N, 3.41. Red crystals suitable for X-ray analysis were grown by slow evaporation from a CH_2Cl_2 solution at 300 K.

Synthesis of $[Re_2(\mu\text{-}OC_6F_5)_2(CO)_6(\mu\text{-pydz})]$ (3). A sample of $[Re(CO)_5OTf]$ (50 mg, 0.105 mmol) dissolved in freshly distilled CH_2Cl_2 was treated at room temperature with 1.5 equiv of C_6F_5OH (30 mg, 0.160 mmol) and 1.5 equiv of DMAN (34 mg, 0.160 mmol). After refluxing for 5 h, IR monitoring showed two ν(CO) bands at 2023 cm^{-1} (s), 1913 cm^{-1} (vs), attributable to $[DMANH]^+[Re_2(\mu\text{-}OC_6F_5)_3(CO)_6]^-$. The colorless solution was evaporated to dryness, dissolved in freshly distilled toluene, treated with 0.5 equiv (with respect to $[Re(CO)_5OTf]$) of pyridazine (4.3 mg, 0.054 mmol), and refluxed for 3 h. The color of the solution turned to dark yellow and IR monitoring showed the disappearance of the bands of the intermediate species, substituted by the bands of **3**. ^1H NMR analysis in CD_2Cl_2 of the reaction mixture showed the presence mainly of **3**, accompanied by minor amounts of unidentified species. Separation by column chromatography on SiO_2 using dichloromethane/hexane 9:1 afforded spectroscopically pure **3** (R_F = 0.64). Isolated yields: 22 mg (47%). IR ν(CO) (cm^{-1}), CH_2Cl_2: 2047 w, 2033 s, 1944 s, 1916 s; ^1H NMR (δ, CD_2Cl_2): 9.85 (pseudo t, 2H), 8.27 (pseudo t, 2H); ^{19}F NMR (δ, CD_2Cl_2, 173 K): −156.7 (pseudo d, *ortho*), −161.8 (pseudo d, *ortho*), −163.7 (pseudo t, *meta*), −164.3 (pseudo t, *meta*), −164.3 (pseudo t, *para*). UV−vis (CH_2Cl_2) λ = 360 nm (7.5×10^3 cm^{-1} M^{-1}). Anal. Calcd: C, 26.78; H, 0.41; N, 2.84. Found: C, 26.92; H, 0.48; N, 2.89. Yellow crystals suitable for X-ray analysis were grown by slow diffusion of *n*-hexane into a CH_2Cl_2 solution, at 248 K.

Synthesis of $[Re_2(\mu\text{-}OC_6H_5)_2(CO)_6(\mu\text{-pydz})]$ (4). Molten phenol was used as the solvent, as follows: a sample of $[Re(CO)_5OTf]$ (60 mg, 0.126 mmol) was treated in a Schlenk tube with C_6H_5OH (6 g), 0.65 equiv of pyridazine (6.6 mg, 0.082 mmol), 0.9 equiv of Na_2CO_3 (12 mg, 0.113 mmol), and then heated at 55 °C, causing melting of phenol. The orange mixture was maintained at this temperature for 20 h, and then unreacted C_6H_5OH was sublimed under vacuum, leaving a yellow-orange residue. The solid was suspended in THF, then the mixture was filtered and chromatographed on SiO_2, with dichloromethane/ethyl acetate (9:1). The expected product **4** was eluted first (R_F = 0.73, isolated yield 11 mg, 20%.) IR ν(CO) (cm^{-1}), CH_2Cl_2: 2036 w, 2021 s, 1927 s, 1903 s; ^1H NMR (δ, CD_2Cl_2): 9.83 (pseudo t, 2H), 8.20 (pseudo t, 2H), 7.31−7.26 (m, 4H), 7.00−6.92 (m, 6H). UV−vis (CH_2Cl_2) λ = 372 nm (6.9×10^3 cm^{-1} M^{-1}). Anal. Calcd: C, 32.75; H, 1.75; N, 3.47. Found: C, 32.58; H, 1.59; N, 3.53. Yellow crystals for X-ray analysis were obtained by slow diffusion of *n*-hexane into a CH_2Cl_2 solution, at 248 K.

Synthesis of $[Re_2(\mu\text{-}OCH_3)_2(CO)_6(\mu\text{-pydz})]$ (5). A sample of $NEt_4[Re_2(\mu\text{-}OCH_3)_3(CO)_6]$ (43 mg, 0.057 mmol) dissolved in 5 mL of freshly distilled CH_2Cl_2, was treated with 1 equiv of pyridazine (4.4 mg, 0.057 mmol) and 1 equiv of triflic acid CF_3SO_3H (8.5 mg, 0.057 mmol). The mixture was stirred at room temperature for 6 h, than the orange-red solution was evaporated to dryness. Separation by column chromatography on SiO_2 using dichloromethane/ethyl acetate (9:1) afforded, besides the expected $[Re_2(\mu\text{-}OCH_3)_2(CO)_6(\mu\text{-pydz})]$ (R_F = 0.71, compound **5**), also two other species in which the methoxo groups had been partially or completely replaced by OH groups: $[Re_2(\mu\text{-}OCH_3)(\mu\text{-OH})(CO)_6(\mu\text{-pydz})]$ (R_F = 0.24) and $[Re_2(\mu$-

dx.doi.org/10.1021/ic202284a | Inorg. Chem. 2012, 51, 2966−2975

$OH)_2(CO)_6(\mu$-pydz)] (R_F = 0.14, compound **6**: it was isolated by elution with neat ethyl acetate). [$Re_2(\mu$-$OCH_3)_2(CO)_6(\mu$-pydz)] (**5**). Isolated yield: 16 mg (41%). IR ν(CO) (cm^{-1}), CH_2Cl_2: 2027 w, 2010 s, 1915 s, 1892 s; ^{1}H NMR (δ, CD_2Cl_2): 9.69 (pseudo t, 2H), 8.06 (pseudo t, 2H), 4.22 (s, 6H). UV−vis (CH_2Cl_2) λ = 370 nm (8.6×10^3 cm^{-1} M^{-1}). Anal. Calcd: C, 21.11; H, 1.48; N, 4.10. Found: C, 20.94; H, 1.37; N, 4.10.

Synthesis of [$Re_2(\mu$-$OH)_2(CO)_6(\mu$-pydz)] (6). A sample of [$Re_4(\mu_3$-$OH)_4(CO)_{12}$] (150 mg, 0.131 mmol) dissolved in 3 mL of water was treated with 2 equiv of pyridazine (21.0 mg, 0.262 mmol) and heated at 100 °C for 4 h in a microwave oven, affording an orange precipitate and a yellow solution. The entire suspension was chromatographed on a SiO_2 column, with ethyl acetate/dichloromethane (1:1), affording spectroscopically pure **6**. Isolated yield: 111 mg, 65%. IR ν(CO) (cm^{-1}), CH_2Cl_2: 2029 w, 2013 s, 1917 s, 1892 s; ^{1}H NMR (δ, CD_2Cl_2): 9.75 (pseudo t, 2H), 8.07 (pseudo t, 2H), 1.14 (s, 2H). UV−vis (CH_2Cl_2) λ = 368 nm (8.0×10^3 cm^{-1} M^{-1}). EI-HRMS: m/z 655.923460, calcd for $C_{10}H_6N_2O_8Re_2$: 655.923945. Anal. Calcd: C, 18.35; H, 0.92; N, 4.28. Found: C, 18.56; H, 1.04; N, 4.21.

Single-Crystal X-ray Diffraction Analysis. *Crystal Data for* ***2***·CH_2Cl_2. $C_{23}H_{16}Cl_2N_2O_6Re_2S_2$, M_r = 923.80, orthorhombic, space group *Pbca* (No. 61), a = 18.041(2) Å, b = 14.442(2) Å, c = 20.886(2) Å, V = 5441.8(11) Å^3, Z = 8, d_{calc} = 2.255 g cm^{-3}, T = 100(2) K, crystal size = 0.35 mm × 0.27 mm × 0.23 mm, μ = 9.281, λ = 0.71073 Å. Refinement of 334 parameters on 7883 independent reflections out of 68 104 measured reflections (R_{int} = 0.0346, R_σ = 0.0191, $2\theta_{max}$ = 60.0°) led to R_1 = 0.0231 ($I > 2\sigma(I)$), wR_2 = 0.0545 (all data), and S = 1.087, with the largest peak and hole of 0.940 and −0.610 e Å^{-3}.

Crystal Data for ***3***. $C_{22}H_4F_{10}N_2O_8Re_2$, M_r = 986.67, orthorhombic, space group *Fdd*2 (No. 43), a = 19.395(2) Å, b = 25.618(2) Å, c = 10.262(2) Å, V = 5098.8(12) Å^3, Z = 8, d_{calc} = 2.571 g cm^{-3}, T = 150(2) K, crystal size = 0.14 mm × 0.11 mm × 0.11 mm, μ = 9.613, λ = 0.71073 Å. Refinement of 199 parameters on 3694 independent reflections out of 27 975 measured reflections (R_{int} = 0.0606, R_σ = 0.0374, $2\theta_{max}$ = 60.0°) led to R_1 = 0.0243 ($I > 2\sigma(I)$), wR_2 = 0.0507 (all data), and S = 1.017, with the largest peak and hole of 0.894 and −0.635 e Å^{-3}.

Crystal Data for ***4***·$^1/_2CH_2Cl_2$. $C_{22.5}H_{15}ClN_2O_8Re_2$, M_r = 849.21, monoclinic, space group $P2_1/c$ (No. 14), a = 8.860(2) Å, b = 12.518(2) Å, c = 23.094(2) Å, β = 96.10(2)°, V = 2546.8(7) Å^3, Z = 4, d_{calc} = 2.215 g cm^{-3}, T = 295(2) K, crystal size = 0.19 mm × 0.07 mm × 0.05 mm, μ = 9.650, λ = 0.71073 Å. Refinement of 325 parameters on 7447 independent reflections out of 57 778 measured reflections (R_{int} = 0.0540, R_σ = 0.0303, $2\theta_{max}$ = 60.0°) led to R_1 = 0.0313 ($I > 2\sigma(I)$), wR_2 = 0.0635 (all data), and S = 1.019, with the largest peak and hole of 0.985 and −0.731 e Å^{-3}.

CCDC-830740−830742 contains the crystallographic data for **2**−**4**. These data can be obtained free of charge from The Cambridge Crystallographic Data Centre.

Computational Details. Ground-state geometries were optimized by means of density functional calculations. The parameter-free hybrid functional PBE0[20] was employed along with the standard valence double-ζ polarized basis set 6-31G(d,p) for C, H, Cl, N, and O. For Re and S, the Stuttgart−Dresden effective core potentials were employed, along with the corresponding valence triple-ζ basis set.

All the calculations were done assuming C_{2v} (for **3**−**6**) or C_2 (for **2**) symmetry. The nature of all the stationary points was checked by computing vibrational frequencies and all the species were found to be true minima.

In order to simulate the absorption electronic spectrum down to 230 nm, the lowest 50 singlet excitation energies were computed by means of time-dependent density functional calculations. Calculations were done also in the presence of solvent (toluene, used in most of the photophysical characterizations), as described by the conductor-like polarizable continuum model (CPCM).[21]

All the calculations were done with Gaussian 03.[22]

Electrochemical Measurements. The cyclovoltammetric analysis has been performed at scan rates typically ranging from 0.02 V s^{-1} to 10 V s^{-1}, in HPLC-grade acetonitrile solutions at 0.00025−0.001 M concentration in each substrate, deareated by N_2 bubbling, with 0.1 M tetrabutylammonium hexafluorophosphate (TBAPF$_6$, Fluka) as the supporting electrolyte, at 298 K. The ohmic drop has been compensated by the positive feedback technique.[23] The experiments were carried out using an AUTOLAB PGSTAT potentiostat (EcoChemie, The Netherlands) run using a personal computer (PC) with GPES software. The working electrode was a glassy carbon one (AMEL, diameter = 1.5 mm) cleaned by diamond powder (Aldrich, diameter = 1 μm) on a wet cloth (STRUERS DP-NAP); the counterelectrode was a platinum wire; the reference electrode was an aqueous saturated calomel electrode, having, in our working medium, a difference of −0.385 V vs the $Fc^+|Fc$ couple (the intersolvental redox potential reference currently recommended by IUPAC)[24] and +0.032 V vs the $Me_{10}Fc^+|Me_{10}Fc$ couple (an improved intersolvental reference under investigation).[25] The normalized convoluted peak currents have been computed by the relationship

$$\frac{i_L}{c} = \frac{I_L}{Ac} = nFD^{1/2}$$

where I_L is the limiting current, i_L the limiting current density, A the electrode surface, c the substrate concentration in the bulk, n the number of transferred electrons, F the Faraday constant (F = 96485 C mol^{-1} e^{-1}), and D the diffusion coefficient. The pseudo-first-order k' constants for the chemical reaction of the P product of the first monoelectronic oxidation step have been estimated from the following equations:

$$\ln\left(\frac{[P]_t}{[P]_0}\right) = -k't = \ln\left(\frac{I_{p,b}}{I_{p,f}}\right)$$

where

$$t = \frac{(E_\lambda - E_{p,f}) + (E_\lambda - E_{p,b})}{v}$$

Here, $E_{p,f}$ is the peak potential of the forward peak, $I_{p,f}$ the current of the forward peak, $E_{p,b}$ the peak potential of the backward peak, $I_{p,b}$ the current of the backward peak, E_λ the inversion potential in the positive potential scan, and v the potential scan rate.

Photophysical Measurements. Steady-state fluorescence measurements and quantum yield determinations have been performed on a Cary eclipse fluorescence spectrometer (Varian, Inc., Agilent Technologies, Santa Clara, CA). The solutions have been prepared under N_2 directly in the quartz cuvettes, using the Schlenk technique, and were further deoxygenated by bubbling N_2 for 20 min just before measurements. The emission intensities have been normalized to an absorption value of 0.1. Quantum yields have been determined by comparison with the emission of [$Ru(bpy)_3$]Cl_2 in water (Φ = 0.04).[26]

Dynamic fluorescence measurements have been performed with a frequency modulated phase fluorometer (Digital K2, I.S.S., Urbana, IL). The excitation was accomplished by the 9 mW output of a 378-nm diode laser (I.S.S., Urbana, IL). At least 15 data points at logarithmically spaced frequencies in the range of 0.3−30 MHz with a cross-correlation frequency of 400 Hz (A2D, ISS, Inc., USA) have been acquired for lifetime measurements. The convenient accuracies for phase angles and modulation ratios have been 0.2° and 0.004, respectively. Lifetime measurements have been performed under the magic-angle conditions[27] and a 535-nm long-pass filter (Andover Co.) has been employed in order to cut light scattering. A solution of glycogen in doubly distilled water has been used as a reference sample.[28] Lifetime data fitting has been accomplished by an ISS routine, based on the Marquardt least-squares minimization, with a two-exponential decay scheme, in order to take into account the scattering contribution to the overall signal. The fit of the fluorescence intensity decay ($F(t)$) yields the lifetime values τ_i, together with the corresponding fractional intensities (f_i):

$$F(t) = \sum \alpha_i \, e^{-t/\tau_i}$$

dx.doi.org/10.1021/ic202284a | Inorg. Chem. 2012, 51, 2966−2975

and

$$f_i = \frac{\alpha_i \tau_i}{\sum \alpha_i \tau_i}$$

where α_i represents the pre-exponential factors.

■ ASSOCIATED CONTENT

Supporting Information

Three tables with details concerning the computations and the electrochemical characterization; 10 figures showing details about the NMR spectra, the crystal structures, the isodensity surfaces of some relevant molecular orbitals, the electrochemical parameters, the absorption spectra in dichloromethane, and the EGL correlation; crystallographic data in CIF format, and optimized coordinates in Tripos Mol2 format. This material is available free of charge via the Internet at http://pubs.acs.org.

■ AUTHOR INFORMATION

Corresponding Author

*E-mail: monica.panigati@unimi.it.

■ ACKNOWLEDGMENTS

G.D., D.M., and P.M. thank the Italian MIUR for financial support (PRIN 2009 PRAM8L Innovative materials for organic and hybrid photovoltaics).

■ REFERENCES

(1) (a) Fernandez-Moreira, V.; Thorp-Greenwood, F. L.; Coogan, M. P. *Chem. Commun.* **2010**, *46*, 186−202. (b) Lo, K. K.-W. *Top. Organomet. Chem.* **2010**, *29*, 115−158. (c) Lo, K. K.-W.; Hui, W. K.; Chung, C. K.; Tsang, K. H.-K.; Ng, D. C.-M.; Cheung, K.-K. *Coord. Chem. Rev.* **2005**, *249*, 1434−1450.

(2) Yersin, H.; Rausch, A. F.; Czerwieniec, R.; Hofbeck, T.; Fisher, T. *Coord. Chem. Rev.* **2011**, *255*, 2622−2652.

(3) See for instance (a) Kumar, A.; Sun, S.-S.; Lees, A. J. *Top. Organomet. Chem.* **2010**, *29*, 1−35. (b) Yam, V. W.-W.; Wong, K. M.-C. *Chem. Commun.* **2011**, *47*, 11579−11592.

(4) See for instance (a) Villegas, J. M.; Stoyanov, S. R.; Huang, W.; Rillema, D. P. *Inorg. Chem.* **2005**, *44*, 2297−2309. (b) Tseng, Y.-H.; Bhattacharya, D.; Lin, S.-H.; Thanasekaran, P.; Wu, J.-Y.; Lee, L.-W.; Sathiyendiran, M.; Ho, M.-L.; Chung, M.-W.; Hsu, K.-C.; Chou, P.-T.; Lu, K.-L. *Inorg. Chem.* **2010**, *49*, 6805−6807.

(5) (a) Nahhas, A. E.; Cannizzo, A.; van Mourik, F.; Blanco-Rodriguez, A. M.; Záliš, S.; Vlček, A.; Chergui, M. *J. Phys. Chem.* **2010**, *114*, 6361−6369. (b) Baková, R.; Chergui, M.; Daniel, C.; Vlček, A.; Záliš, S. *Coord. Chem. Rev.* **2011**, *255*, 975−989. (c) Gindensperger, E.; Köppel, H.; Daniel, C. *Chem. Commun.* **2010**, *46*, 8225−8227. (d) Kayanuma, M.; Daniel, C.; Köppel, H.; Gindensperger, E. *Coord. Chem. Rev.* **2011**, *255*, 2693−2703.

(6) Panigati, M.; Donghi, D.; D'Alfonso, G.; Mercandelli, P.; Sironi, A.; Mussini, P.; D'Alfonso, L. *Inorg. Chem.* **2006**, *45*, 10909−10921.

(7) Donghi, D.; D'Alfonso, G.; Mauro, M.; Panigati, M.; Mercandelli, P.; Sironi, A.; Mussini, P.; D'Alfonso, L. *Inorg. Chem.* **2008**, *47*, 4243−4255.

(8) Mauro, M.; Quartapelle Procopio, E.; Sun, Y.; Chien, C. H.; Donghi, D.; Panigati, M.; Mercandelli, P.; Mussini, P.; D'Alfonso, G.; De Cola, L. *Adv. Funct. Mater.* **2009**, *19*, 2607−2614.

(9) See Lucenti, E.; D'Alfonso, G.; Macchi, P.; Maranesi, M.; Roberto, D.; Sironi, A.; Ugo, R. *J. Am. Chem. Soc.* **2006**, *128*, 12054−12055 and references therein..

(10) Schmidt, S. P.; Nitschke, J.; Trogler, W. C. *Inorg. Synth.* **1989**, *26*, 113−117.

(11) (a) Ciani, G.; D'Alfonso, G.; Freni, M.; Romiti, P.; Sironi, A. *J. Organomet. Chem.* **1978**, *152*, 85−94. (b) Jiang, C.; Wen, Y.-S.; Liu, L.-K.; Hor, T. S. A.; Yan, Y. K. *Organometallics* **1998**, *17*, 173−181.

(12) Herberhold, M.; Süss, G.; Ellermann, J.; Gäbelein, H. *Chem. Ber* **1978**, *111*, 2931−2941.

(13) Geometric parameters found in **2**−**4** are unexceptional and similar to those reported for analogous species containing a Re−(μ-OR)−Re or a Re−(μ-SR)−Re fragment (Cambridge Structural Database 5.32). Bond distances and angles reported in the text are average values; the largest standard uncertainty on bond distances and angles are 0.012 Å and 0.5°, respectively.

(14) The C_{2v} geometry of **2** possesses two imaginary frequencies (34*i* and 31*i*). This conformation resides 4.6 kJ mol^{-1} higher than the C_2 minimum. In addition, starting the optimization from the solid-state geometry an asymmetric minimum was found, whose energy is only negligibly different from those of the C_2 minimum. Since MO energies and excitations are almost identical for the C_2 and the C_1 conformers, only the values computed for the symmetric species will be reported and discussed.

(15) (a) Wendt, H.; Bitterlich, S. *Electrochim. Acta* **1992**, *37*, 1951−1958. (b) Said, A. H.; Mhalla, F. M.; Amatore, C.; Verpeaux, J. N. *J. Electroanal. Chem.* **1999**, *464*, 85−92. (c) Said, A. H.; Mhalla, F. M.; Amatore, C.; Thouin, L.; Pebay, C.; Verpeaux, J. N. *J. Electroan. Chem.* **2002**, *537*, 39−46.

(16) (a) Swain, C. G.; Lupton, E. C. Jr. *J. Am. Chem. Soc.* **1968**, *90*, 4328−4337. (b) Hansch, C.; Leo, A.; Taft, R. W. *Chem. Rev.* **1991**, *91*, 165−195.

(17) Giordano, P. J.; Wrighton, M. S. *J. Am. Chem. Soc.* **1979**, *101*, 2888−2897.

(18) (a) Benkstein, K. D.; Hupp, J. T.; Stern, C. L. *Inorg. Chem.* **1998**, *37*, 5404−5405. (b) Woessner, K. D.; Helms, J. B.; Shen, Y.; Sullivan, B. P. *Inorg. Chem.* **1998**, *37*, 5406−5407. (c) Marimaran, B.; Rajendran, T.; Lu, Y. L.; Lee, G. H.; Peng, S. M.; Lu, K. L. *J. Chem. Soc., Dalton Trans.* **2001**, 515−517. (d) Marimaran, B.; Thanasekaran, P.; Rajendran, T.; Lin, R. J.; Chang, I. J.; Lee, G. H.; Peng, S. M.; Rajagopal, S.; Lu, K. L. *Inorg. Chem.* **2002**, *42*, 5323−5325.

(19) Quartapelle Procopio, E.; Mauro, M.; Panigati, M.; Donghi, D.; Mercandelli, P.; Sironi, A.; D'Alfonso, G.; De Cola, L. *J. Am. Chem. Soc.* **2010**, *132*, 14397−14399.

(20) Called PBE1PBE in Gaussian. (a) Adamo, C.; Barone, V. *J. Chem. Phys.* **1999**, *111*, 6158−6170. (b) Perdew, J. P.; Burke, K.; Ernzerhof, M. *Phys. Rev. Lett.* **1996**, *77*, 3865−3868. (c) Perdew, J. P.; Burke, K.; Ernzerhof, M. *Phys. Rev. Lett.* **1997**, *78*, 1396.

(21) (a) Barone, V.; Cossi, M. *J. Phys. Chem. A* **1998**, *102*, 1995−2001. (b) Cossi, M.; Barone, V. *J. Chem. Phys.* **2001**, *115*, 4708−4717. (c) Cossi, M.; Rega, N.; Scalmani, G.; Barone, V. *J. Comput. Chem.* **2003**, *24*, 669−681.

(22) Gaussian 03 (revision C.02), Gaussian, Inc., Wallingford, CT, 2004.

(23) Bard, A. J.; Faulkner, L. R. *Electrochemical Methods. Fundamentals and Applications*; Wiley: New York, 2002, pp 648−650.

(24) (a) Gritzner, G.; Kuta, J. *Pure Appl. Chem.* **1984**, *56*, 461−466. (b) Gritzner, G. *Pure Appl. Chem.* **1990**, *62*, 1839−1858.

(25) (a) Noviandri, I.; Brown, K. N.; Fleming, D. S.; Gulyas, P. T.; Lay, P. A.; Masters, A. F.; Phillips, L. *J. Phys. Chem. B* **1999**, *103*, 6713−6722. (b) Ruiz, J.; Astruc, D. *C. R. Acad. Sci., Sér. IIc: Chem.* **1998**, *I*, 21−27. (c) Falciola, L.; Gennaro, A.; Isse, A. A.; Mussini, P. R.; Rossi, M. *J. Electroanal. Chem.* **2006**, *593*, 47−56.

(26) Ishida, H.; Tobita, S.; Hasegawa, Y.; Katoh, R.; Nozaki, K. *Coord. Chem. Rev.* **2010**, *254*, 2449−2458.

(27) Lakowicz, J. R. *Principles of Fluorescence Spectroscopy*, 2nd ed.; Kluwer Academic/Plenum Publishers: New York, 1999.

(28) Collini, M.; Chirico, G.; Baldini, G.; Bianchi, M. E. *Biopolymers* **1995**, *36*, 211−225.